CMS Draft Analysis Note

2012/01/13
Head Id: 40099
Archive Id: 40222M
Archive Date: 2011/02/18
Archive Tag: trunk

Search for Long-Lived Particles using Displaced Photons in pp Collisions at $\sqrt{(s)} = 7\,\text{TeV}$

Daniele Del Re, Shahram Rahatlou, Michael Sigamani, and Livia Soffi
INFN Sezione di Roma "La Sapienza", Rome, Italy

Abstract

We present the results of a search for long-lived particles decaying into photons in $\sqrt{(s)} = 7\,\text{TeV}$ proton-proton collisions. We use the Missing Transverse Energy and the time of impact of the photon on the surface of the ECAL to search for an excess of events over our SM background prediction. After our signal selection, using a data set of 4.55 ± 0.2 fb^{-1}, we see no significant excess over our background prediction and proceed to set limits on the production cross-section of $\tilde{\chi}_1^0 \to \gamma\tilde{G}$ at 95% C.L. and place a lower limit of XXX GeV/c^2 on the mass the $\tilde{\chi}_1^0$.

1 Introduction

The Standard Model (SM) of particle physics has proven extremely successful, but despite its many successes, still remains incomplete. Theoretical motivations provide compelling rationale for searches into the production and decay of long-lived particles decaying into final state photons with Missing Transverse Energy ($\not\!\!E_{\mathrm{T}}$) as evidence for physics beyond the SM. Of particular theoretical interest are supersymmetry (SUSY) models with gauge-mediated SUSY-breaking (GMSB) [1]. These models have been long been studied as candidates for new physics beyond the TeV energy scale, and coupled with the relatively high production cross section and striking experimental signature allow for discoveries using early LHC data.

Many versions of these models employ a similar phenomenology, we therefore, choose a benchmark scenario as our search model. This scenario is commonly described as the 'Snowmass Slope and Parameter Set 8' (SPS8) [2]. In this scenario the neutralino ($\tilde{\chi}_1^0$) is the next-to-lightest supersymmetric particle and decays almost exclusively into a photon (γ) and a weakly interacting stable gravitino ($\tilde{G}$). The $\tilde{G}$ in this case is the lightest supersymmetric particle (LSP), and gives rise to Missing Transverse Energy ($\not\!\!E_{\mathrm{T}}$) by leaving the detector without depositing energy. Assuming R-parity conservation, we expect pairwise production of the $\tilde{\chi}_1^0$. Futhermore, the $\tilde{G}$ becomes a promising dark matter candidate, which has theorized mass in the range $0.5 < m_{\tilde{G}} < 1.5$ keV$/c^2$. We note that the most stringent limits with the benchmark GMSB model on the mass of the $\tilde{\chi}_1^0$ to are greater than 149 GeV/c^2 [3].

Our study will therefore focus on the search for neutral long-lived particles decaying into photons. The main feature of this signature is that the daughter photons will be produced from a displaced vertex, and will be detected by the ECAL at relatively large times. In the case of no significant excess observed above known SM processes, we will set about estimating an upper-limit on the Branching Fraction times cross-section of the $\tilde{\chi}_1^0 \rightarrow \tilde{G}\gamma$ decay. Important variables in this study are the measured time of impact of the photon on the surface of the ECAL, the shape of the energy deposit on the ECAL (since off-pointing photons will produce a more elongated cluster shape in the ECAL with respect to prompt photons), the $\not\!\!E_{\mathrm{T}}$, and also the number of jets above a particular energy threshold.

2 Datasets and Trigger

2.1 Data

The data analyzed in this note corresponds to an integrated luminosity of 4.55 ± 0.2 fb^{-1}, collected and reconstructed using `CMSSW_4_2_3`. Only luminosity-sections certified as GOOD in the official good run file were used and the datasets analysed correspond to:

189.4 pb^{-1}: `/Photon/Run2011A_May10ReReco-v1/AOD`
884.2 pb^{-1}: `/Photon/Run2011A_PromptReco-v4/AOD`
326.3 pb^{-1}: `/Photon/Run2011A_05Aug2011-v1/AOD`
637.9 pb^{-1}: `/Photon/Run2011A_PromptReco-v6/AOD`
2517.8 pb^{-1}: `/Photon/Run201_PromptReco-v1/AOD`
JSON: `Cert_160404-180252_7TeVPromptReco_Collisions11_JSON.txt`

2.2 Background and signal Monte Carlo

The Monte Carlo (MC) events used in this analysis are generated at centre of mass energy $\sqrt{s} = 7$ TeV with Summer 2011 prescriptions and have been processed using `CMSSW_4_2_3`.

Furthermore, the MC is generated using PYTHIA [4] and processed with a simulation of the CMS detector using the GEANT4 package [5]. This is with the exception of the $t\bar{t}$ MC, which is generated using TAUOLA [6]. The QCD multi-jet and γ+jet MC datasets are generated in a wide $\hat{P_T}$ range[1]. The event sample size for each $\hat{P_T}$ bin, the cross section (σ) at the leading order (LO) and the equivalent integrated luminosity are listed in Table 1.

For our signal, approximately 50,000 events per parameter-point were requested for our GMSB signal MC. The generation follows line 8 of the SPS8 proposal, where the free parameters, the SUSY breaking scale (Λ), and the $\tilde{\chi}_1^0$ lifetime ($c\tau$) are varied to cover an appropriate range of phase space. These are documented in Table 2 along with their respective cross-sections. Depending on the SUSY breaking scale 8%–30% of the GMSB signal also decay as $\tilde{\chi}_1^0 \to \gamma Z$.

Process	Kinematic cut [GeV]	σ_{LO} [pb]	No. events	$\mathcal{L}$ [pb]$^{-1}$
QCD	$50 < \hat{P_T} < 80$	6.4×10^6	2.5×10^7	3.9
QCD	$80 < \hat{P_T} < 120$	7.8×10^5	3.5×10^7	4.4×10
QCD	$120 < \hat{P_T} < 170$	1.1×10^5	5.1×10^6	4.6×10
QCD	$170 < \hat{P_T} < 300$	2.4×10^4	1.1×10^7	4.5×10^2
QCD	$300 < \hat{P_T} < 470$	1.1×10^3	1.5×10^7	1.4×10^4
QCD	$470 < \hat{P_T} < 600$	7.0×10	1.9×10^7	1.4×10^5
QCD	$600 < \hat{P_T} < 800$	1.5×10	2.7×10^7	1.8×10^6
QCD	$800 < \hat{P_T} < 1000$	1.8	3.1×10^7	1.7×10^6
γ+jet	$50 < \hat{P_T} < 80$	2.7×10^4	1.1×10^7	4.1×10^2
γ+jet	$80 < \hat{P_T} < 120$	4.5×10^3	7.5×10^6	1.7×10^3
γ+jet	$170 < \hat{P_T} < 300$	2.3×10	2.0×10^6	8.7×10^4
γ+jet	$300 < \hat{P_T} < 470$	1.5	3.6×10^6	2.4×10^6
γ+jet	$470 < \hat{P_T} < 800$	1.3×10^{-11}	9.5×10^6	7.3×10^{17}
γ+jet	$1400 < \hat{P_T} < 1800$	1.3×10^{-5}		
$t\bar{t}$	-	9.4×10	8.0×10^5	8.5×10^3
$W \to e\nu$	-	7.9×10^3	5.1×10	6.4×10^2

Table 1: The description of the background MC samples used in this analysis

Λ [GeV]	$c\tau$ [mm]	σ_{LO} [pb]
100	1, 250, 500, 1000, 2000	0.2357
120	1, 250, 500, 1000, 2000	0.0860
140	1, 250, 500, 1000, 2000	0.0368
160	1, 250, 500, 1000, 2000	0.0181
180	1, 250, 500, 1000, 2000	0.0092

Table 2: The description of the signal GMSB MC samples used in this analysis

2.3 Trigger

The primary triggers used for our search is `Photon75_CaloIdVL_IsoL` (runs 160410-165120) and `Photon90_CaloIdVL_IsoL` (runs 165121-178421), `Photon90EBOnly_CaloIdVL_IsoL_TriPFJet25` (178421-180252). All of which are seeded using the `L1_SingleEG20`. The first two of these triggers have an online requirement of $\sigma_{i\eta i\eta} < 0.024$, ECAL Iso/$E_t(\gamma) < 0.2$, HCAL Iso (isolation)/$E_t(\gamma) < 0.2$, and $H/E < 0.15$ and P_T greater than 75 and 90 GeV. The last trigger has additional requirements of $\eta < 1.4$ and three or more Particle-Flow (PF) [7] jets above 25 GeV/c. All offline selection cuts are chosen to be tighter than the HLT selection. We see from Figure 1 that `Photon90_CaloIdVL_IsoL` becomes 100% efficient with an offline cut of $P_T(\gamma) > 100$ GeV.

[1] where $\hat{P_T}$ is the transverse momentum of one of the two partons in the rest frame of the hard process

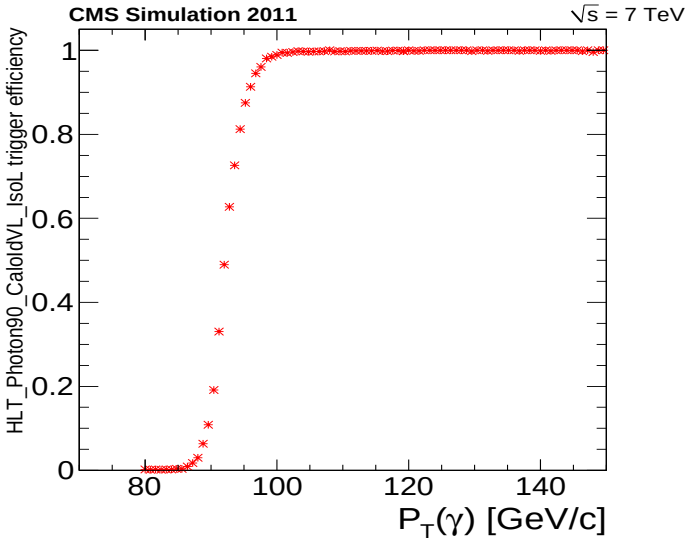

Figure 1: The trigger efficiency turn-on for `Photon90_CaloIdVL_IsoL`

3 Reconstruction and Event Selection

The event selection for this analysis requires at least one high P_T isolated photon with at least three jets in the final state. The motivation the requirement on jets comes from a 2010 study performed to optimise the GMSB expected exclusion limits.The main backgrounds for this analysis arise from SM processes which give rise to mis-identified photons and mis-measured $\not{E}_T$. These include QCD events which can mimic the signature of $\tilde{\chi}_1^0 \rightarrow \tilde{G}\gamma$ decay due to the mis-reconstruction of photons and the presence of fake $\not{E}_T$. Requirements on calorimeter and track isolation are used to reduce this contribution. Alongside the QCD background we also have a γ+jet background. This is an important background for this analysis due to the presence of a real isolated prompt photon in the final state, with fake $\not{E}_T$ expected due to the mis-reconstruction of photons from jets. Although the presence of a real, high P_T, isolated photon can mimic the signature of the signal, the event topology is very different between γ+jet and GMSB signal events, therefore, we see that γ+jet events are characterised by a lower jet multiplicity with respect to our signal. A requirement on the minimum number of jets above a P_T threshold is demonstrated to reject a large fraction of this background.

Alongside the processes which give rise to fake $\not{E}_T$ we have a real $\not{E}_T$ contribution from Electroweak (EWK) decays. These include $W \rightarrow e\nu$, where the lepton can fake the presence of a photon, and the ν giving rise to real $\not{E}_T$. We also expect some contribution from $t\bar{t}$ decays where the top quark decays almost 100% of the time into a W boson with a b quark. The W boson then decays to leptons which can produce a $\gamma+\not{E}_T$ signature, with the $\not{E}_T$ arising due to one or more neutrinos. To estimate the contribution from these backgrounds we use MC simulations normalised to the CMS theoretical cross section.

Finally, we also expect events which do not originate from proton-proton collisions. These backgrounds are made up of cosmic rays, beam-halo muons, and ECAL spikes. Since the reconstructed time can be large for these events, they represent an important background in this analysis. These backgrounds are reduced significantly by requiring a good vertex, 3 or more jets in the event, and the (CSC tight) halo-cleaning recipe outlined in [8].

The characteristic shape of an off-pointing photon cluster can be exploited to identify the decay products of a long-lived particle. Hense, we use the S_{Minor} variable, which represent the minor

axis of the ellipse for the ECAL cluster. This variable has been previously used to discriminate energy deposits from photons and neutral pions. We reduce a large fraction of cosmic rays by requiring a primary vertex, with at least four associated tracks (vndof), whose position (d_0) is less than 2 cm from the centre of CMS in the direction transverse to the beam and 24 cm in the direction along the beam ($|z|$) in each event.

3.1 Pre-selection

For the next iteration of the analysis we planned on using a RECO skim on the `Photon` dataset based on our current pre-selection definition. This will give us access to the `PixelVeto` requirement shown to be effective at vetoing EWK events. We will also have access to the full `RecHit` collection as opposed to the reduced collection. Our pre-selection definition is as follows:

- $P_T(\gamma) > 70\,\text{GeV}$;
- $(\text{HCAL Iso}/P_T(\gamma) + \frac{H}{E}) \times E(\gamma) < 6.0$;
- $0.1 < S_{Minor} < 0.53$;
- Good Vertex (vndof ≥ 4,$d_0 < 2$, $|z| < 24$).

One can see from Table 4 that the `Photon` dataset is reduced to around 5% of the original value using our pre-selection. This is well within the recommended values for skims outlined by the Primary Dataset Working Group.

3.2 Pile-up

We re-weight the MC by the number of pile-up (PU) interactions taken from the MC truth following the recommended re-weighting schemes outlined in [9] and [10]. In Figure 2 we see the S_{Minor} and S_{major} distributions overlaid for different values of number of primary vertices. These distributions are central to our off-pointing photon reconstruction and we see that they are not affected significantly with increased PU. Also, from Figure 3 we note that the GMSB signal selection efficiency does not depreciate significantly with increased PU. Furthermore, the variables in Figure 3 show an efficiency of above 90% up to 15 primary vertices apart from the p_T TRK Isolation (Iso). However, the efficiency still remains at a reasonable level.

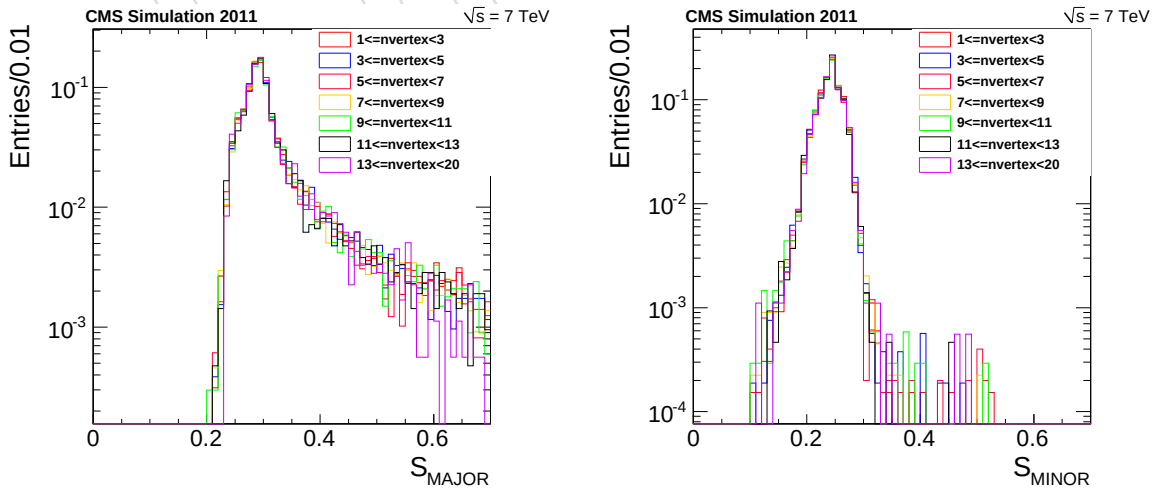

Figure 2: The S_{Minor} (left) and S_{Major} (right) distributions overlaid for different values of number of primary vertices for the GMSB signal ($\Lambda = 100\,\text{GeV}$, $c\tau = 250\text{mm}$).

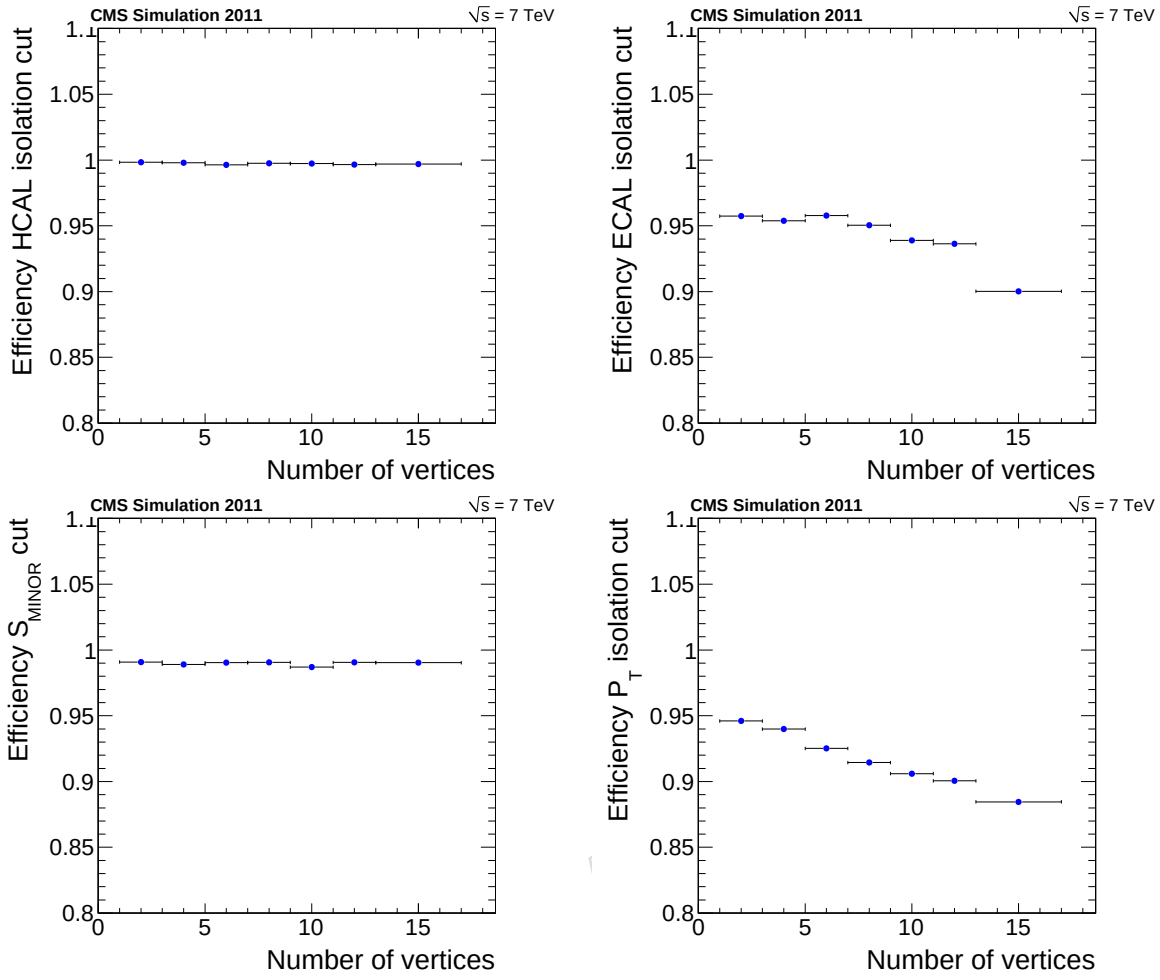

Figure 3: The HCAL Iso (top left), ECAL Iso (top right), S_{Minor} (bottom left), and TRK Iso (bottom right) cut efficiency for the GMSB signal ($\Lambda = 100\,\text{GeV}$, $c\tau = 250\text{mm}$) plotted against the number of primary vertices.

3.3 Photon reconstruction

The photon reconstruction begins with the identification of energy deposits in the ECAL according to dedicated supercluster algorithms. These algorithms are discussed in detail in Ref. [11]. In order to retrieve the ECAL timing information lost through we reconstruct our photon candidates from unclean superclusters with the energy, momentum, cluster shape and isolation variables then calculated using the photon candidate. One should note that the `PixelVeto` information is not available in the unclean AOD sample, and we therefore see an increase in the EWK contribution.

Since photons from the decay of the $\widetilde{\chi}_1^0$ are expected to have a larger P_T spectrum compared to photons from SM backgrounds, this remains an important variable in distinguishing between signal and background for this analysis. In order to reduce our background we require some HCAL, ECAL, and tracking isolation (cone size 0.4) for our photon candidates. We also place absolute thresholds as well as relative thresholds on the HCAL and ECAL isolation cuts in order to prevent requirements which are tighter than the noise level of the calorimeters. These isolation requirements are shown to be very efficient in rejecting QCD events. We find that $t\bar{t}$ events are heavily suppressed by tracking isolation, however, γ+jet events are not rejected as

easily using isolation cuts due to the presence of a real isolated photon in the final state. In order to reduce the γ+jet contribution, we veto events where the leading jet back to back to photon, so

- $\Delta R(\gamma, jet) > 2/3$, where $\Delta R = \sqrt{(\phi_\gamma - \phi_{jet})^2 + (\eta_\gamma - \eta_{jet})^2}$;
- and $0.7 < p_T^{jet}/p_T^\gamma < 1.3$.

We use S_{Minor} to identify energy deposits in the ECAL compatible with isolated photons, and apply standard CMS cuts to select events compatible with proton-proton collisions. We apply the standard topological cuts ($E6/E2 > 0.04$ and $E4/E1 > (0.04 * log(E1) - 0.024)$ to reject events compatible with spikes. Furthermore, to reject 'scraping' events produced by the interaction of beam-related protons with the LHC collimators, the fraction of tracks classified as high purity must exceed 20%. We veto events consistent with anomalous HCAL noise not due to instrumentation issues according to recommendations from the HCAL Detector Performance Group (DPG) [12].

Lastly, we only consider barrel photons in this analysis and veto photons found in trigger tower 32 of supermodule -16, which is known to have unreliable timing measurements. Overall, we see a reasonable agreement between data and MC for the selection variables used in this analysis (see Figure 4-6. In some variables one can note some over/under estimation between data and MC, which further motivates the use of data-driven estimates for our main backgrounds (discussed in Section 4).

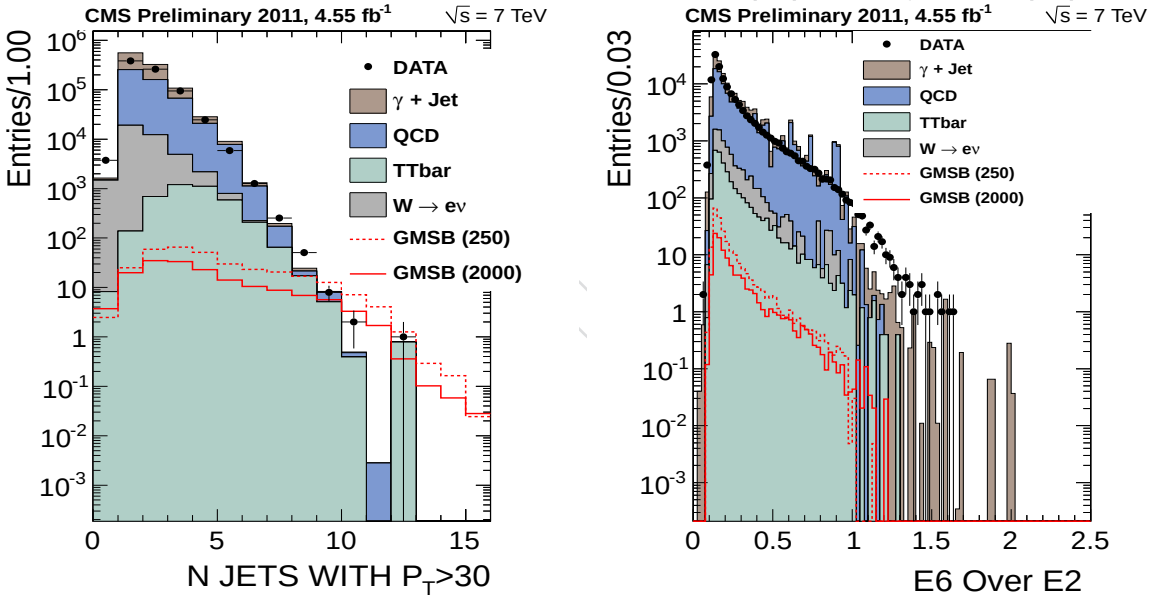

Figure 4: The distribution of the number of reconstructed jets with $P_T > 30$ GeV (left) and $E6/E2$ (right) with at least 3 jets above $P_T > 30$ for data and MC normalized to the luminosity of data after photon ID.

The selection requirements for photons are listed as 'tight' in Table 3. The 'loose' is used later in our QCD data-driven control sample (CS) estimation. The selection criteria differs from the recipe described by the `EGamma` group, where the motivation for this can be found in [13] which focuses on using cluster shape variable in displaced photon searches. The selection efficiencies for our selection cuts can be seen in Table 4.

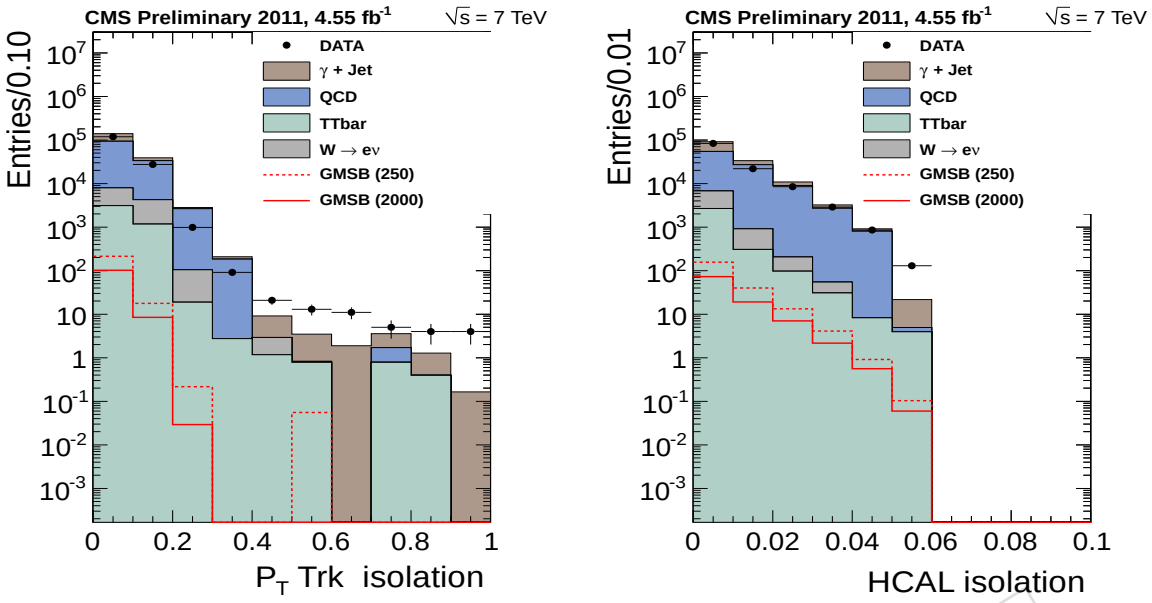

Figure 5: The distribution of $\sum P_T/P_T\,(\gamma)$ (left) and $\sum P_T$ (right) with at least 3 jets above $P_T > 30$ (right) for data and MC normalised to the luminosity of data after photon ID.

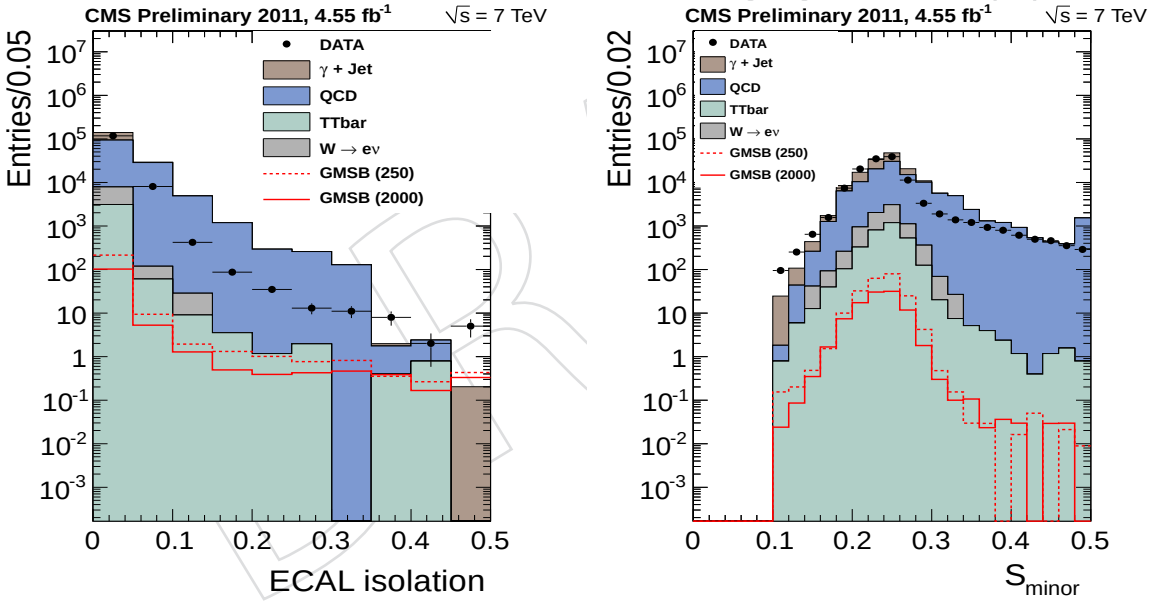

Figure 6: The distribution of $\sum \mathrm{ECAL/E}\,(\gamma)$ (left) and S_{Minor} (right) with at least 3 jets above $P_T > 30$ for data and MC normalised to the luminosity of data after photon ID.

3.4 Jet reconstruction

The number of jets above a P_T threshold can be used as discriminating variable between GMSB signal and background, where a P_T threshold on the jet allows for rejection of jets which do not originate from the fragmentation of prompt quarks. We reconstructed our jets using PF with anti-kt 5 [14] algorithm. We require $\mathrm{Jet}_{p_T} > 30$ GeV/c, and the jet to be non-overlapping to photons ($\Delta R(\gamma, jet) > 0.5$).

Criteria	Requirement (tight)	Requirement (loose)
$\|\eta\|$	< 1.4	
$P_T(\gamma)$	> 100 GeV	
Halo Veto	CSC Tight	
S_{Minor}	$0.15 < S_{Minor} < 0.3$	$0.15 < S_{Minor} < 0.3$
Topological	E6/E2 and swiss-cross	
ECAL time	> -2.0 ns	
HCAL Iso	$\{ \sum HCAL/E(\gamma) < 0.05$ and $\sum HCAL < 2.4$ GeV	$\{ \sum HCAL/E(\gamma) < 0.1$ and $\sum HCAL < 4$ GeV
ECAL Iso	$\{ \sum ECAL/E(\gamma) < 0.05$ and $\sum ECAL < 2.4$ GeV	$\{ \sum ECAL/E(\gamma) < 0.1$ and $\sum ECAL < 4.5$ GeV
TRK Iso	$\{ \sum P_T/P_T(\gamma) < 0.1$	$\{ \sum P_T/P_T(\gamma) < 0.2$

Table 3: The loose and tight photon ID selection criteria

%	γ+jet	QCD	$t\bar{t}$	$W \to e\nu$	GMSB (250)	GMSB (2000)	Data
Pre-selection	49	0.29	4.3	0.88	61	37	6.5
$P_T(\gamma)$	19	14	37	24	63	54	43
$N_{jets} \geq 3$	10	17	79	12	82	65	16
$\|\eta\|$	73	86	86	76	92	93	82
Halo Veto	100	100	100	100	100	100	99
ECAL time	100	100	100	100	100	100	99
S_{Minor}	99	67	96	98	99	98	88
HCAL Iso	99	99	99	99	99	99	99
ECAL Iso	98	62	85	97	90	89	91
Topological	92	97	98	96	93	93	93
P_T Iso	89	76	72	60	93	92	81
Not γ+jet	96	99	99	99	100	99	99
ϵ_{TOT}	0.52	0.0019	0.71	0.0096	20.5	9.6	0.13

Table 4: The efficiencies for the selection criteria on data and MC. GMSB 250 corresponds to $\Lambda = 100$, $c\tau = 250$ mm and GMSB 2000 corresponds to $\Lambda = 100$, $c\tau = 2000$ mm.

Furthemore, clean-up for PF Jets was studied using the procedure outlined in [15], requiring energy fractions on PF jets for neutral and charged hadrons. Any disagreement between data and MC arises due to calorimeter noise, spikes, and beam-related backgrounds. Side-band cuts are then applied in the regions of disagreement improving the overall agreement between data and MC. However, in Figure 7 we see a good overall agreement between data and MC therefore we conclude that jet cleaning of this kind will not be of benefit in this analysis.

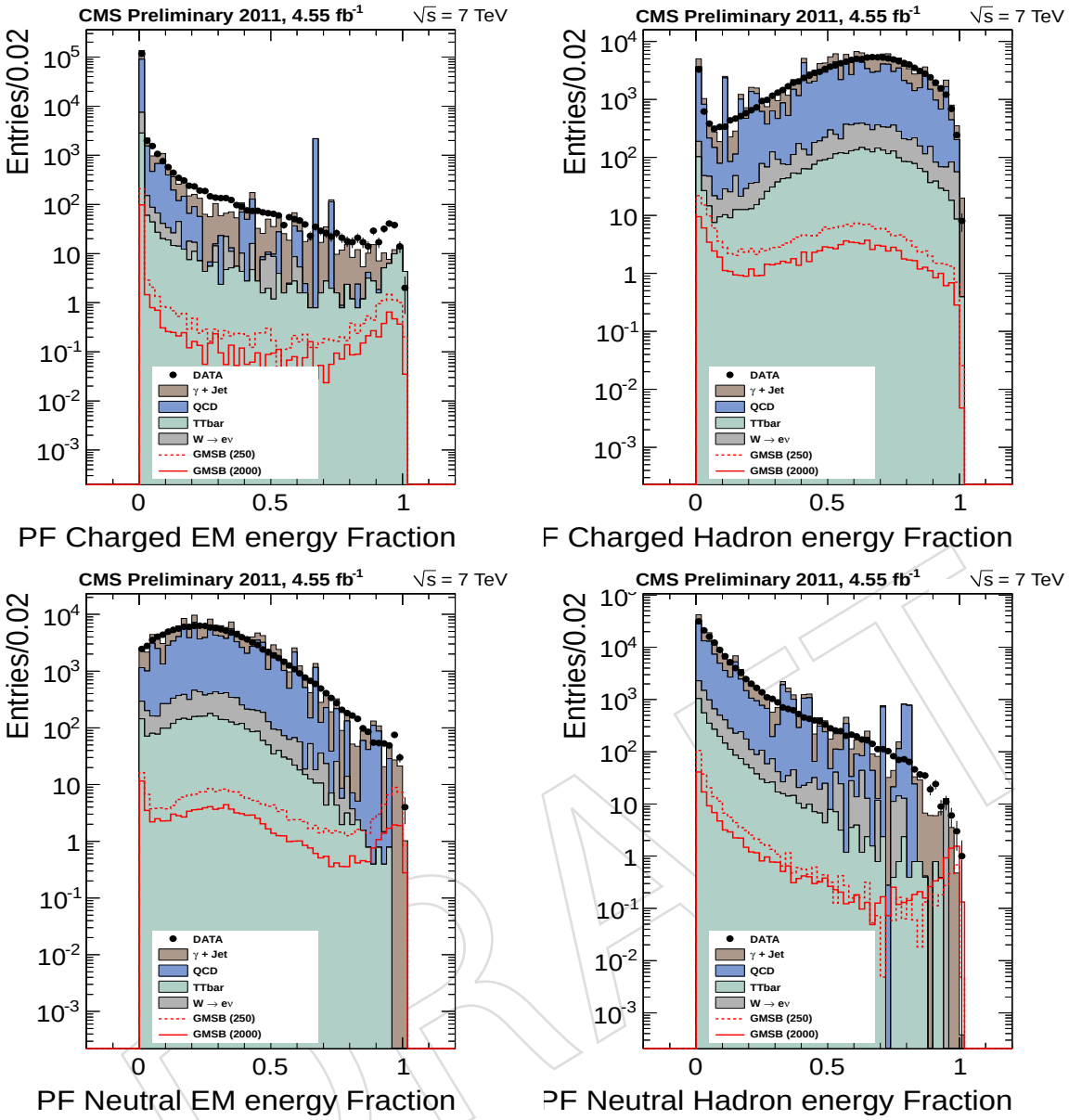

Figure 7: The distribution of the Jet electromagnetic (top left) and hadronic (top right) energy fractions from charged and particles. The distributions of the Jet electromagnetic (bottom left) and hadronic (bottom right) energy fractions from neutral particles.

3.5 ECAL timing and $\not\!\!E_T$ reconstruction

For large regions of the signal parameter space where the $\tilde{\chi}_1^0$ is assumed to have a non negligible lifetime, the ECAL time becomes an important variable in identifying a delayed γ. This is also the case for the $\not\!\!E_T$ as used in most SUSY analyses. Therefore we use these two variables in order to discriminate our signal from the expected backgrounds. From Figure 14 we see that the $\not\!\!E_T$ and ECAL time for different values of the $\tilde{\chi}_1^0$ lifetime show no significant correlation. Since the shape of the $\not\!\!E_T$ distribution does not change significantly with the $\tilde{\chi}_1^0$ lifetime.

The $\not\!\!E_T$ energy vector is computed as the opposite of the transverse-momentum sum of all the particles and is reconstructed using the PF algorithm. The ECAL time is calculated using

gaussian fit to the time of impact of all of the RecHits within the supercluster associated to our signal photon. Due to effects seen in both data and MC, a general offset away from zero is seen in the time distribution for both data and MC. In order to correct for this offset, and also to reduce the uncertainty due to the position of the beam-spot and time of interaction, we calibrate our ECAL time measurement event-by-event using the mean time of the event. We start with a general definition for the weighted ECAL time calculation. So

$$\mathrm{T} = \frac{\Sigma \frac{T_i}{\sigma_i^2}}{\Sigma \frac{1}{\sigma_i^2}}, \tag{1}$$

where i are all of the RecHits in the calculation (above 1 GeV threshold), and σ_i is the energy dependent uncertainty on the time measurement outlined in [16]. For the mean time of the event (T_{mean}), i, are all of the RecHits in the event excluding those that belong to the two most energetic photons (our signal candidates). For the signal ECAL time calculation (T_{sig}), i, are all of the RecHits belonging to our signal photon. A gaussian fit is then performed to the resulting distributions of both T_{mean} and T_{sig} (see Figure 16) to extract the mean value and the width. Since the time of collision will vary event-by-event we attempt to remove this dependance (correcting the offset and improving the timing resolution) by using a corrected timing T_{corr}, where

$$T_{corr} = T_{sig} - T_{mean}, \tag{2}$$

with the uncertainty on T_{corr} is defined as

$$\sigma_{T_{corr}} = \sqrt{\sigma^2_{T_{sig}} - \sigma^2_{T_{mean}}} \simeq \sigma_{T_{mean}} \tag{3}$$

One can see the energy (and η) dependence for the offset and resolution of the ECAL timing in Figures 17-20 (appendix). Furthermore, we veto the most energetic RecHit from the time calculation if it is of energy above the gain threshold (130 GeV). From Figure 21 (appendix) one can see that this removes the energy dependence seen in the offset. We also apply a bin-by-bin smearing of the ECAL time distribution in MC to match data using the difference measured in Figure 22.

Lastly, after recommendations from the ECAL DPG, an uncertainty of 0.5 ns has been agreed to be a conservative estimate to use for the total uncertainty on the ECAL timing. This value is derived from Figure 19 (left) where one sees the maximum offset calculated is 0.5 ns.

4 Estimation of backgrounds

The importance of data-driven background determinations in SUSY searches arises from the difficulty in modelling the tails of the QCD background, in predicting cross-sections for the SM backgrounds reliably, and in predicting kinematic distributions such as the number of jets accurately. Therefore, data-driven techniques are employed as much as possible in the estimation of backgrounds. Electroweak backgrounds such as $W \rightarrow e\nu$, and $t\bar{t}$ present similar challenges, but are not as extreme as that of QCD, and γ+jet. Therefore, we estimate these using MC scaled to the luminosity of data. As mentioned previously, for the next iteration of this analysis we plan to use a RECO skim giving us access to the `PixelVeto` which should reduce the EWK contribution.

4.1 Data-driven QCD

The shape of $\not\!\!E_{\mathrm{T}}$ and the ECAL time for QCD events is estimated selecting events which pass the loose selection but fail the tight described in Table 3 (and more than 3 or more jets). Other methods were also tested, however, the method described above gives the best results. The closure test for our background estimation is shown in Figure 8, where we require a good agreement between MC in our standard and control sample selections. The normalisation in these plots are to the area of data. The EWK contribution is estimated to be less than 1% for this control sample. In our closure test one can notice a deviation in data with respect to the MC for the $\not\!\!E_{\mathrm{T}}$ estimate. The agreement between MC in the standard and control sample selections, however, is good which leads us to believe that the shape of the $\not\!\!E_{\mathrm{T}}$ from our data control sample estimate is reliable in spite of this. Furthermore, as mentioned previously clean-up for PF Jets was studied as a possible source for this disagreement. Figure 9 shows that this is not the case.

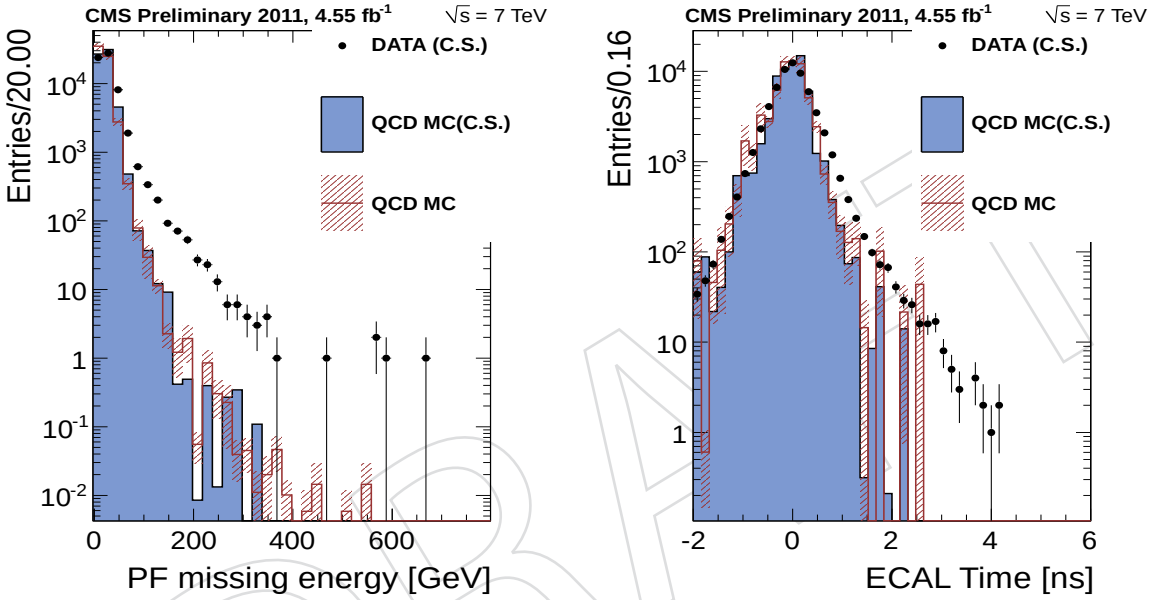

Figure 8: The distribution of the $\not\!\!E_{\mathrm{T}}$ (left) and timing (right) for the data-driven QCD estimate

4.2 Data-driven γ+jet

The shape of $\not\!\!E_{\mathrm{T}}$ and the ECAL time for γ+jet events is estimated selecting events where:

- One photon passes the selection described in Table 3
- We have less than three jets
- The most energetic jet (jet1) is back to back with respect to the photon
- $0.7 < p_T^{jet1}/p_T^{\gamma} < 1.3$
- $p_T^{jet2}/p_T^{\gamma} < 0.1$

We expect resolution effects from the jet reconstruction to behave differently between our final and CS selections, and to be most visible in the ΣE_T distribution. Therefore, we try to account for this by re-weighting our data CS and standard MC (MC passing our final selection) using weights calculated from the ratio of the ΣE_T distribution in γ+jet MC CS (passing the control sample selection) to the standard γ+jet MC. In Figure 15 we show the distributions for the $\not\!\!E_{\mathrm{T}}$

and the ECAL time before re-weighting and also the associated ΣE_T plots. The closure test for our background estimation is shown in Figure 9 where we see a good agreement. Both data CSs are uncorrelated, with the QCD requiring 3 or more jets, whereas the γ+jet requires less than 3 jets. The EWK contribution is estimated to be around 10% for this control sample.

Above run 178421, we use the pre-scaled `Photon90_CaloIdVL_IsoL` trigger for the γ+jet CS, where as for our QCD CS (and final data sample) we use the `Photon90EBOnly_CaloIdVL_IsoL_TriPFJet25` trigger. This is due to the three jet requirement on the latter which is impossible to use given the 'less than three jet' requirement we have for our γ+jet CS.

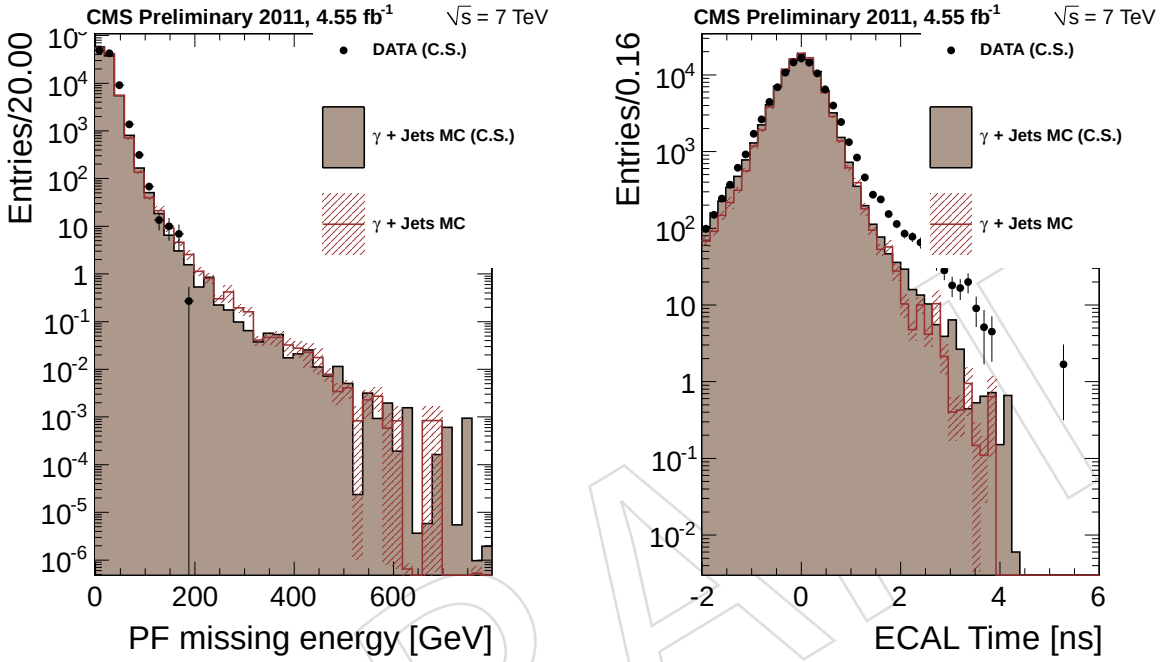

Figure 9: The distribution of the $\not\!\!E_{\mathrm{T}}$ (left) and timing (right) of the data-driven γ+jet estimate

5 Systematic Uncertainties

There are several sources of systematic uncertainty which affect the analysis, the most important for this analysis especially in the case of early discoveries where the number of observed events is small, arises from the tails in the resolution of the $\not\!\!E_{\mathrm{T}}$ and ECAL time which can fake the presence of signal events

The uncertainty on the luminosity $\mathcal{L}$ will be propagated as an uncertainty on the measurement of the signal cross section σ, where the current recommended value at 4.5%. The energy response of the calorimeter is less than unity and varies as a function of jet P_T. The purpose of the absolute jet energy correction is to remove this variation making the response unity for all P_T values. This uncertainty for the jet energy scale correction has been estimated to be roughly 4% using γ+jet events [17]. The uncertainty on the photon scale in the barrel is estimated to be 0.6% and based on the final-state radiation measurement with Z [18]. The uncertainty on the $\not\!\!E_{\mathrm{T}}$ scale and resolution uses the conservative estimate of 5% and 10% respectively based on estimations from [19, 20]. The uncertainty on the ECAL time is estimated this by calculating the discrepancy in the ECAL timing performance between the γ+Jet data CS and prompt

GMSB MC as a function of the photon energy. From these studies an uncertainty of 0.5 ns has been agreed by the ECAL DPG to be a conservative estimate. A summary of all the systematic uncertainties are listed in Table 5, whereby the each object is varied within its uncertainty and the relative difference propagated to the expected upper-limit.

Source	Uncertainty on σ_{UL}^{Exp} (%)
Photon energy scale (0.6%)	9%
Jet energy scale (4%)	10%
Jet resolution (10%)	17%
Luminosity (4.5%)	4.5%
$\not\!\!E_{\mathrm{T}}$ scale (5%)	7.1%
$\not\!\!E_{\mathrm{T}}$ resolution (10%)	2.8%
ECAL time uncertainty (0.5 ns)	X%
Total approx.	23.6 %

Table 5: Summary of the systematic uncertainties on the σ_{UL} calculation

6 Results

As mentioned in Section 3.5 we use the $\not\!\!E_{\mathrm{T}}$ and the ECAL time from the ECAL to discriminate GMSB signal from SM background. We will show the agreement of these distributions in this section using the data-driven CS described above overlaid with EWK MC and GMSB signal. Also, we re-weight the ECAL time for MC according to the prescription described in Section 3.5.

6.1 Distribution of $\not\!\!E_{\mathrm{T}}$ and ECAL time

We see in Figure 10 the distribution for these two variables using data and MC after all analysis requirements. We see in Figure 11 the same distributions using our data-driven background estimates. The data-driven estimates are scaled to data using efficiencies calculated from MC with

$$N_{data}^{def} = N_{data}^{CS} \cdot \frac{N_{MC}^{def}}{N_{MC}^{CS}} \tag{4}$$

where N_{data}^{def} and N_{MC}^{def} are the number of events in data and MC before the background CS selection, and N_{data}^{CS} and N_{MC}^{CS} are the number of events in data and MC after the background CS selection. Furthermore, the QCD and γ+jet background in the first bin of the $\not\!\!E_{\mathrm{T}}$ and below 0.5 ns in the ECAL time is scaled to to area of data. Overall we see a fairly good agreement in all of these plots.

6.2 Fit strategy and upper-limit calculation

There is a reasonable agreement seen in 6.1, however to estimate the normalisations for the various components more accurately we use a binned maximum likelihood fit to data. We use MC to describe the PDFs for the $W \to e\nu$ and $\mathrm{t\bar{t}}$ and normalise each to the luminosity of data (these are fixed components in the fit). For the QCD and γ+jet components we take the PDFs from our control samples derived in Section 4 and float as one component fixing the relative normalisation using efficiencies calculated from MC. For the signal we take the PDF from our MC and this is left to float. Therefore, we perform a 2 parameter fit with one constraint (on the

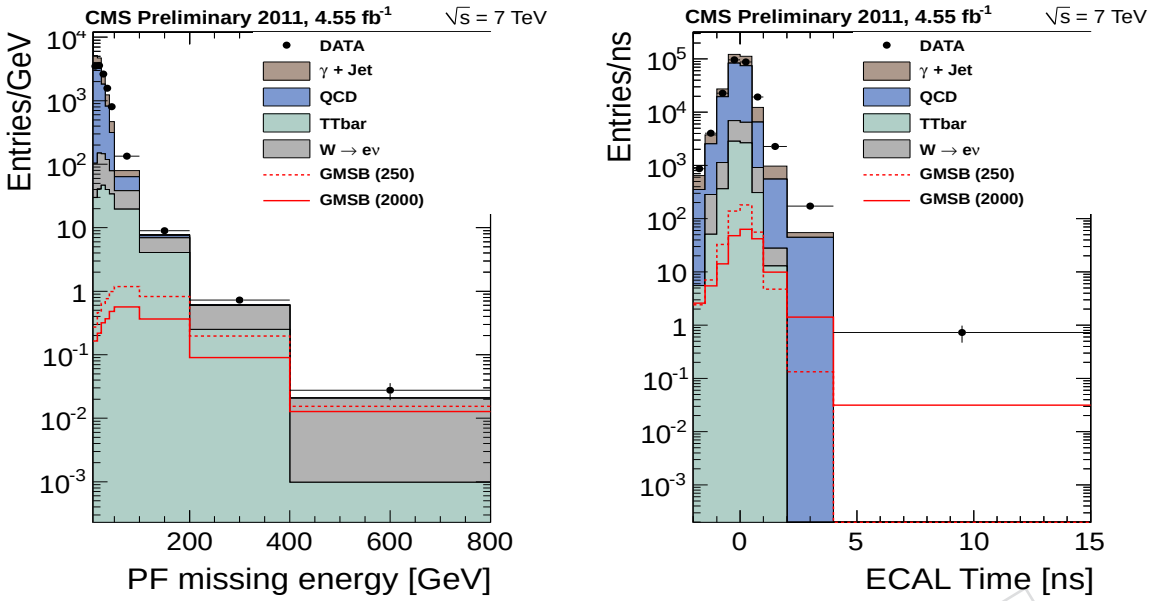

Figure 10: The distribution of the $\not\!\!E_{\mathrm{T}}$ (right) and the ECAL time (left) with at least 3 jets above $P_T > 30$ for data and MC normalised to the luminosity of data after photon ID

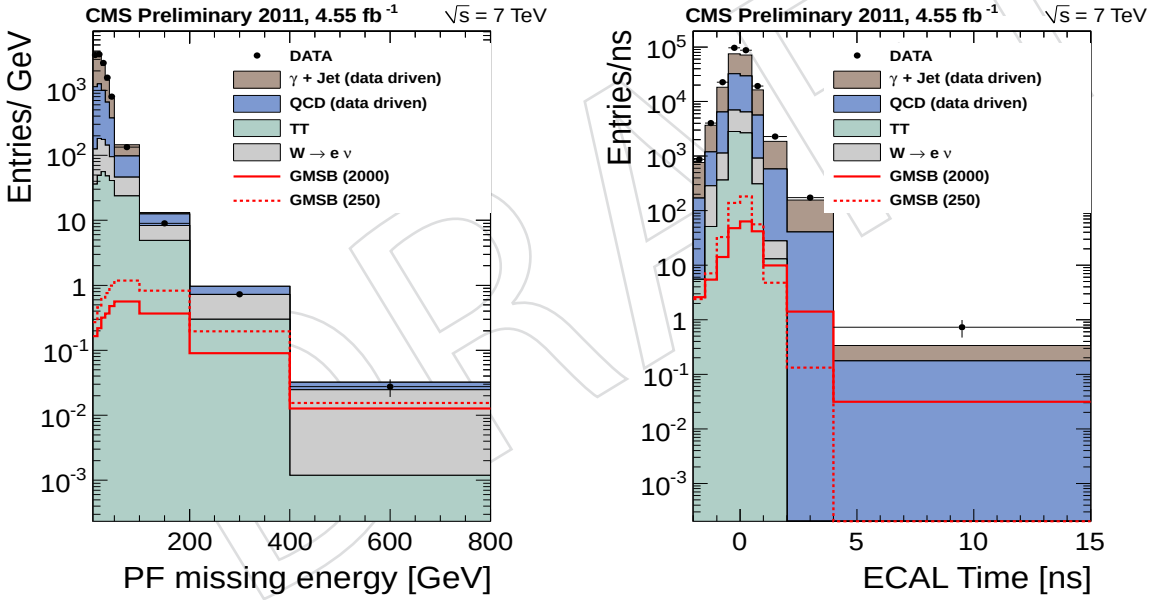

Figure 11: The distribution of the $\not\!\!E_{\mathrm{T}}$ (right) and the ECAL time (left) with at least 3 jets above $P_T > 30$ using the data-driven background CSs described in Section 4

relative normalisation of QCD with respect to γ+jet). The result can be seen in Figure 12 with the respective yields from this plot shown in Table 6.

In order to compute limits we first relate $\tilde{\chi}_1^0$ cross section to N_{GMSB} using the following expression:

$$N_{GMSB} = \mathcal{L} \cdot \epsilon_{GMSB} \cdot \sigma_{GMSB} \tag{5}$$

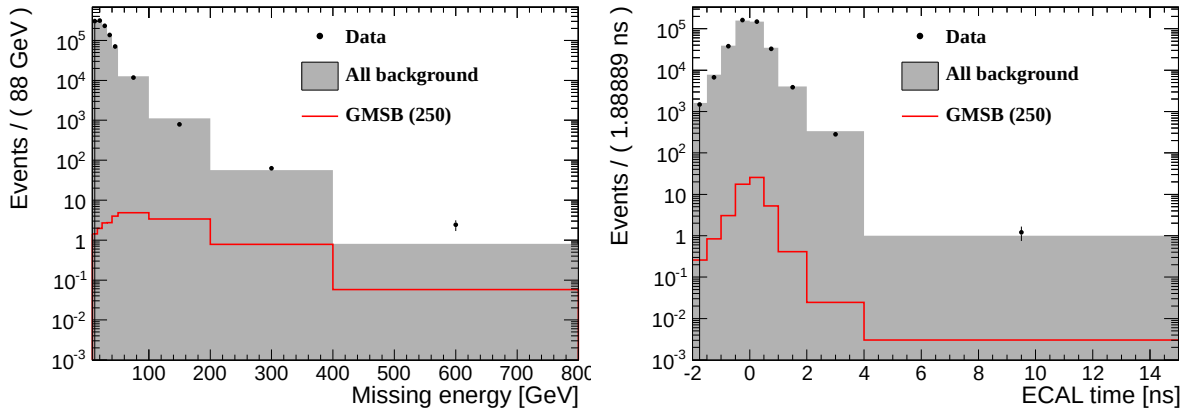

Figure 12: The distributions of $\not\!\!E_{\mathrm{T}}$ (left) and ECAL timing (right) after the final fit for GMSB (250) signal and backgrounds

where $\mathcal{L}$ is the luminosity, and ϵ_{GMSB} is the signal efficiency (taken from Table 4). Using and our fit we attain a liklihood function of the signal GMSB cross-section. Finding the value of the cross-section at the 95% integral gives us our upper-limit at 95% confidence level (CL). The estimated values for the observed and expected (in the assumption of no signal) cross sections at 95% CL are shown in Figure 13. This is repeated for different values of $\tilde{\chi}_1^0$ lifetime, which we the use to construct a 2D exclusion plot for the mass-lifetime plane of the $\tilde{\chi}_1^0$. From this we conclude that we are able to exclude a mass below XXX GeV/c^2 for all the values of the $\tilde{\chi}_1^0$ lifetime considered.

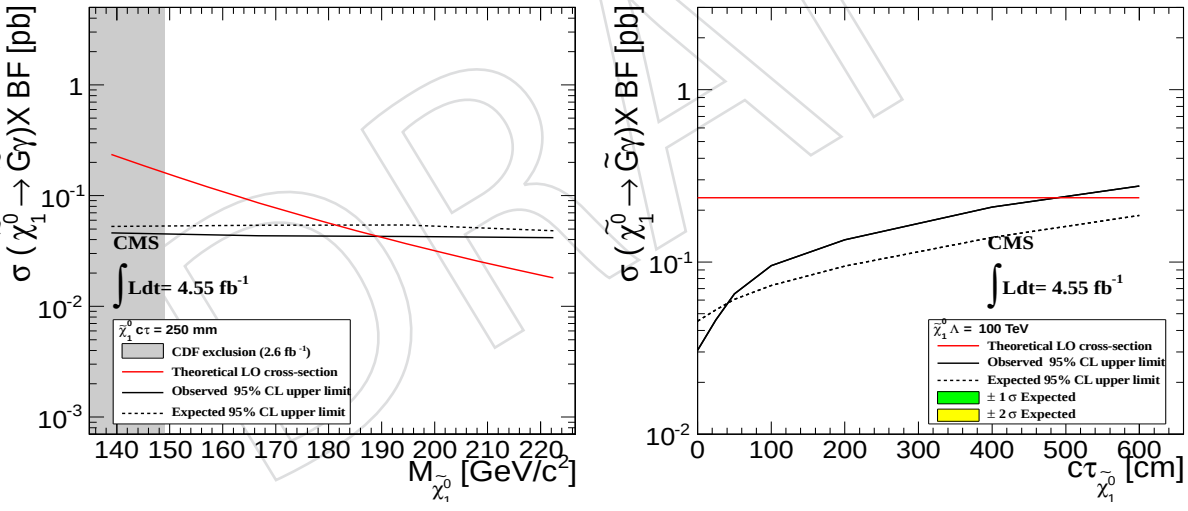

Figure 13: The observed 95% CL cross section upper limits as a function of the $\tilde{\chi}_1^0$ mass for $c\tau = 1$ mm (left), and the $\tilde{\chi}_1^0$ lifetime for $\Lambda = 100$ TeV (right).

	No. Events
QCD	64467 ± 1030
γ+Jet	34005 ± 1012
$t\bar{t}$ (fixed)	3039 ± 55
$W \rightarrow e\nu$ (fixed)	4612 ± 68
GMSB (250)	14 ± 12
GMSB (2000)	25 ± 15
Data	105884 ± 325

Table 6: The final number of events estimated for each component after all selection cuts and the final fit to data

7 Conclusion

In conclusion, we have performed a search for displaced photons using 4.55 ± 0.2 fb^{-1} of CMS collision data at the centre-of-mass energy of 7 TeV. We use the Missing Transverse Energy and timing information from the ECAL to search for an excess of events over our SM background prediction. The data has been found to be in agreement with the expected contributions from Standard Model processes, and limits for the production cross-section of $\widetilde{\chi}_1^0 \rightarrow \gamma\widetilde{G}$ have been estimated. We conclude by placing limits on the production cross-section of $\widetilde{\chi}_1^0 \rightarrow \gamma\widetilde{G}$ at 95% C.L. and place a lower limit of XXX GeV/c^2 on the mass the $\widetilde{\chi}_1^0$.

References

[1] G. F. Giudice and R. Rattazzi, "Theories with gauge-mediated supersymmetry breaking", *Phys. Rept.* **322** (1999) 419–499, arXiv:hep-ph/9801271. doi:10.1016/S0370-1573(99)00042-3.

[2] B. C. Allanach et al., "The Snowmass points and slopes: Benchmarks for SUSY searches", *Eur. Phys. J.* **C25** (2002) 113–123, arXiv:hep-ph/0202233. doi:10.1007/s10052-002-0949-3.

[3] CDF Collaboration, "Search for Supersymmetry with Gauge-Mediated Breaking in Diphoton Events with Missing Transverse Energy at CDF II", *Phys. Rev. Lett.* **104** (2010) 011801, arXiv:0910.3606. doi:10.1103/PhysRevLett.104.011801.

[4] T. Sjostrand, S. Mrenna, and P. Z. Skands, "PYTHIA 6.4 Physics and Manual", *JHEP* **05** (2006) 026, arXiv:hep-ph/0603175. doi:10.1088/1126-6708/2006/05/026.

[5] GEANT4 Collaboration, "GEANT4: A simulation toolkit", *Nucl. Instrum. Meth.* **A506** (2003) 250–303. doi:10.1016/S0168-9002(03)01368-8.

[6] Z. Was, "TAUOLA the library for tau lepton decay, and KKMC/KORALB/KORALZ/... status report", *Nucl. Phys. Proc. Suppl.* **98** (2001) 96–102, arXiv:hep-ph/0011305. doi:10.1016/S0920-5632(01)01200-2.

[7] CMS Collaboration, "Commissioning of the Particle-Flow Reconstruction in Minimum-Bias and Jet Events from pp Collisions at 7 TeV", *CMS PAS PFT-10-002* (2010).

[8] CMS Collaboration, "Beam Halo Event Identification in CMS Using the CSCs, ECAL, and HCAL", *AN-10-111* (2011).

[9] https://twiki.cern.ch/twiki/bin/viewauth/CMS/PileupInformation.

[10] https://twiki.cern.ch/twiki/bin/view/CMS/PileupMCReweightingUtilities.

[11] CMS Collaboration, "Search for New Physics with a Mono-Jet and Missing Transverse Energy in pp Collisions at sqrt(s) = 7 TeV", *EXO-11-003* (2011).

[12] https://twiki.cern.ch/twiki/bin/view/CMS/HcalNoiseInfoLibrary.

[13] CMS Collaboration, "An algorithm for the determination of the flight path of long-lived particles decaying into photons", *EXO-11-212* (2010).

[14] CMS Collaboration, "The anti-kt jet clustering algorithm", *JHEP 0804* (2008) 6374. doi:10.1088/1126-6708/2008/04/063.

[15] CMS Collaboration, "Search for New Physics with Monojet Final States in pp collisions at sqrt(s) = TeV", *AN-11-228* (2011).

[16] CMS Collaboration, "Time Reconstruction and Performance of the CMS Electromagnetic Calorimeter", *JINST* **5** (2010) T03011, arXiv:0911.4044. doi:10.1088/1748-0221/5/03/T03011.

[17] CMS Collaboration, "Determination of the Jet Energy Scale in CMS with pp Collisions at sqrt(s) = 7 TeV", *JME-10-010* (2010).

[18] https://twiki.cern.ch/twiki/bin/viewauth/CMS/VGamma2011.

[19] CMS Collaboration, "MET performance in pp Collisions at sqrt(s) = 7 TeV", *JME-10-009* (2010).

[20] CMS Collaboration, "Search for ADD Extra-dimensions with Photon + MET signature", *AN-11-319* (2011).

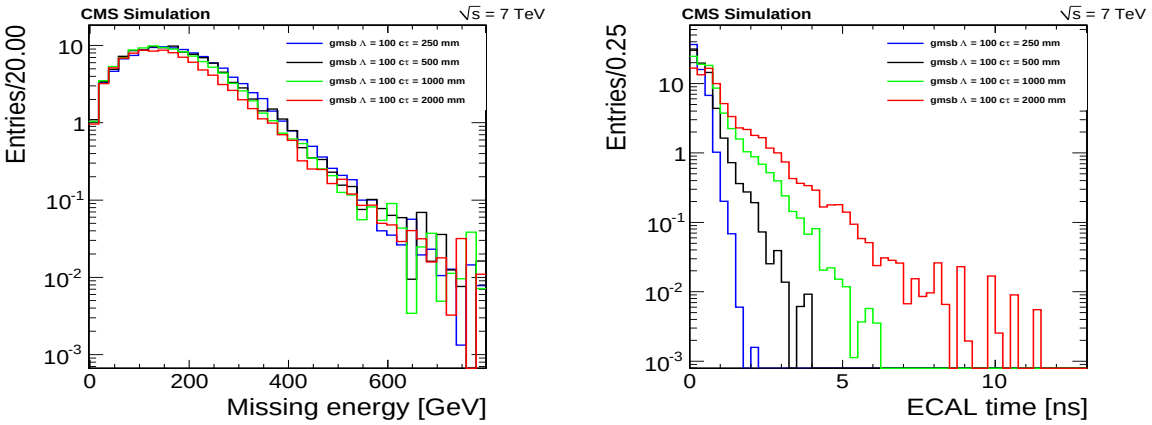

Figure 14: The distribution of the $\not\!\!E_{\mathrm{T}}$ and ECAL time for different GMSB signal points

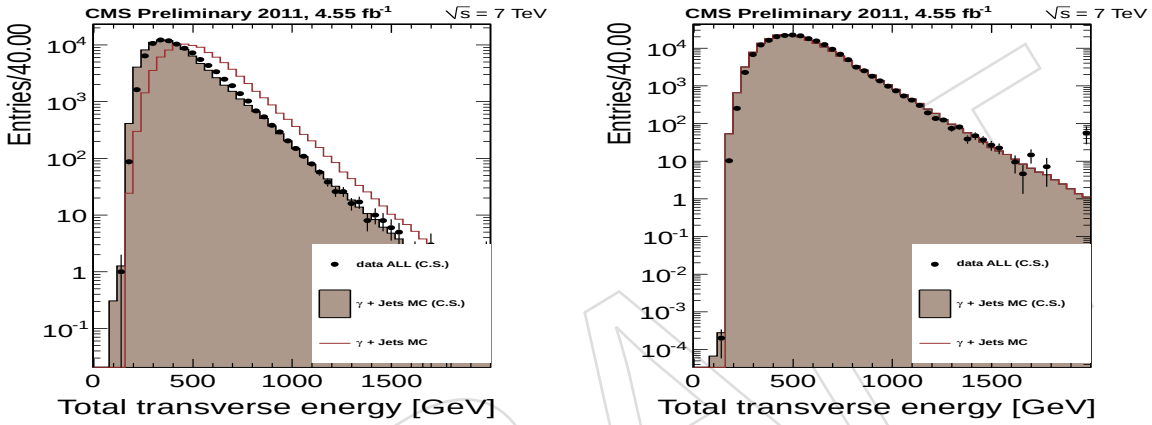

Figure 15: The distribution of the ΣE_T before (left) and after (right) re-weighting.

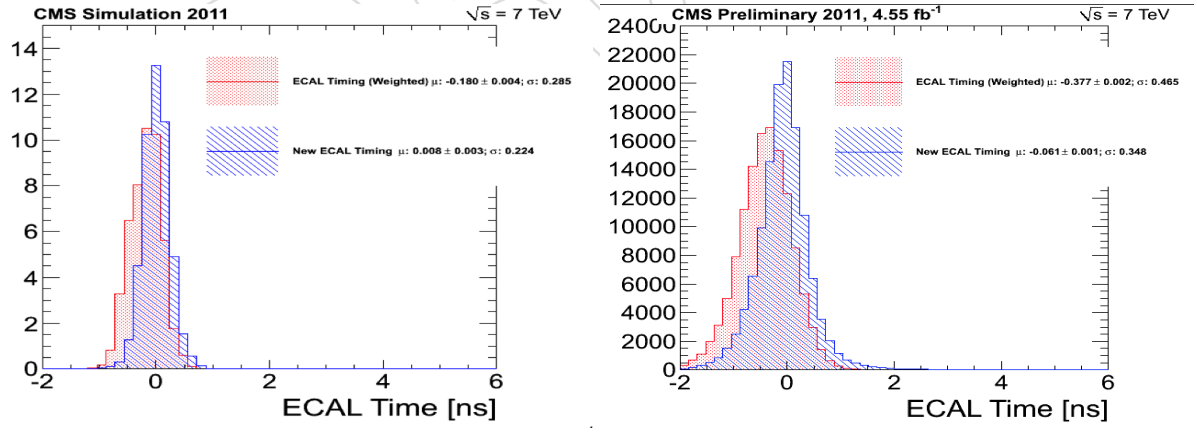

Figure 16: The ECAL time distribution for MC (left) and data (right) before and after the mean time correction.

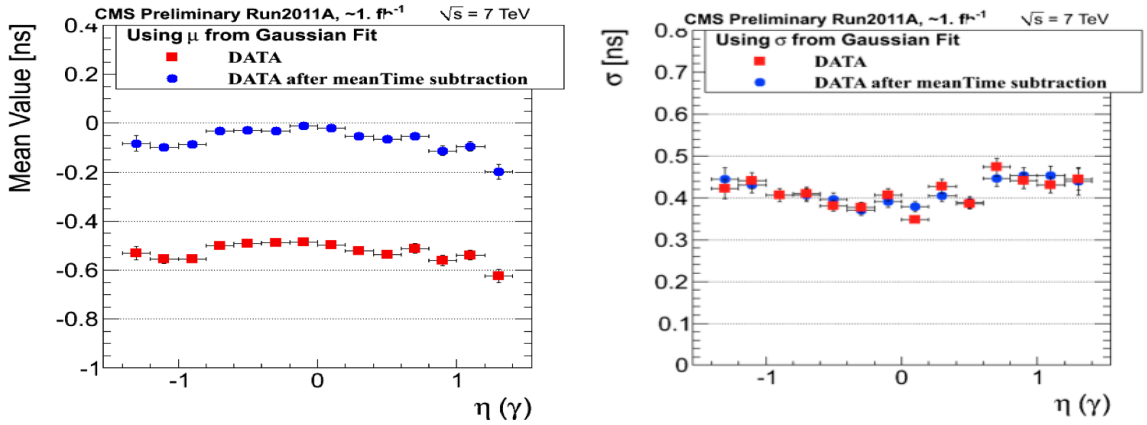

Figure 17: The η dependance of the offset (left) and resolution (right) before and after the mean time correction for data

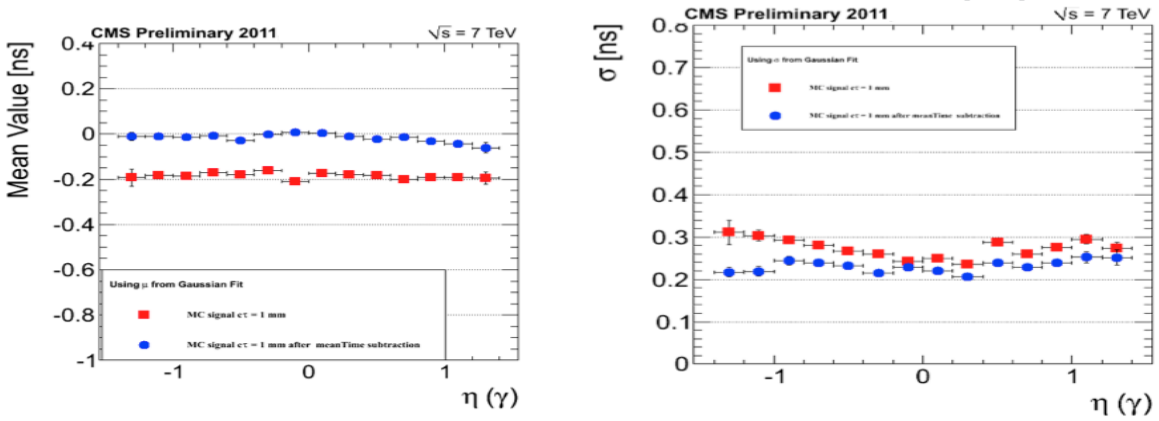

Figure 18: The η dependance of the offset (left) and resolution (right) before and after the mean time correction for MC

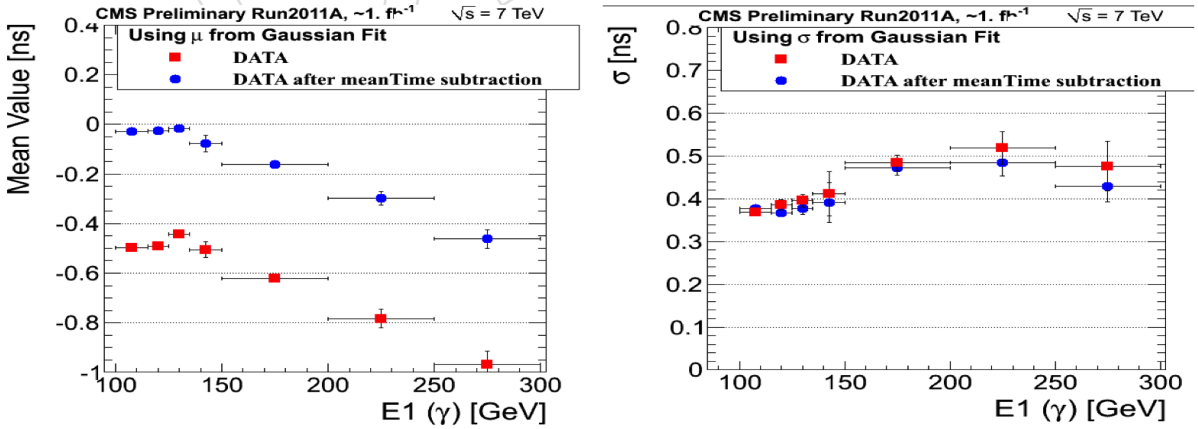

Figure 19: The energy dependance of the offset (left) and resolution (right) before and after the mean time correction for data

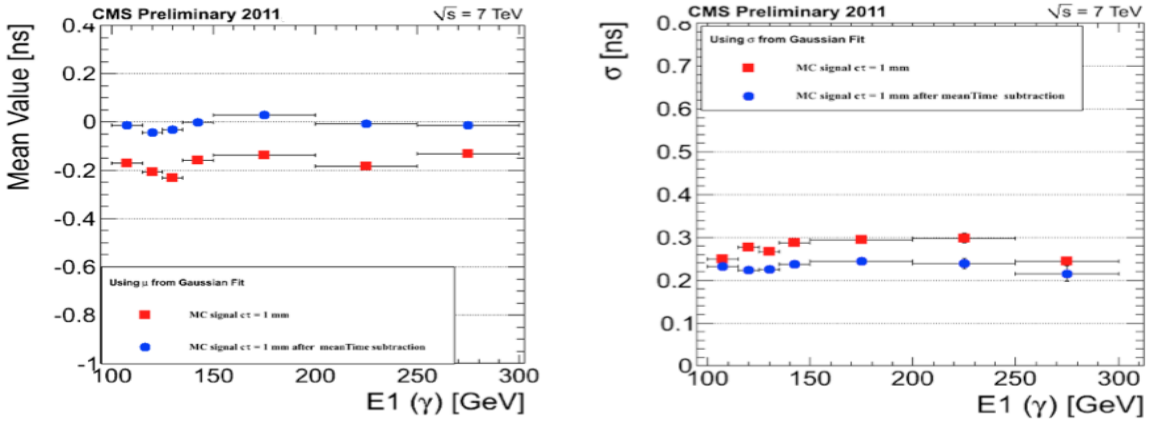

Figure 20: The energy dependance of the offset (left) and resolution (right) before and after the mean time correction for MC

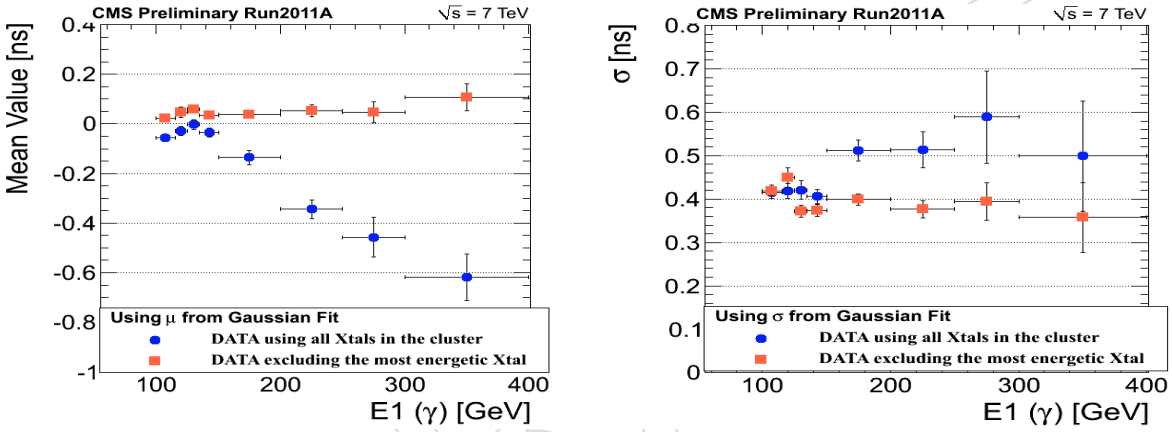

Figure 21: The energy dependance of the offset (left) and resolution (right) before and after mean time and gain switch corrections for data

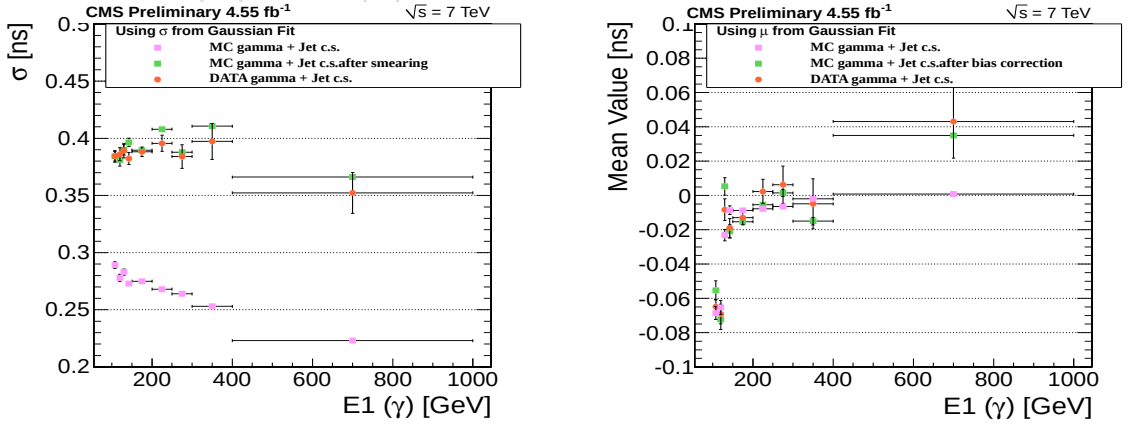

Figure 22: The energy dependant offset (left) and width (right) corrections for data and MC

Dataset name	σ_{LO} [pb]
GMSB_Lambda-100_CTau-1_7TeV_pythia6_cff/Summer11*	0.2357
GMSB_Lambda-100_CTau-250_7TeV_pythia6_cff/Summer11*	0.2357
GMSB_Lambda-100_CTau-500_7TeV_pythia6_cff/Summer11*	0.2357
GMSB_Lambda-100_CTau-1000_7TeV_pythia6_cff/Summer11*	0.2357
GMSB_Lambda-100_CTau-2000_7TeV_pythia6_cff/Summer11*	0.2357
GMSB_Lambda-100_CTau-3000_7TeV_pythia6_cff/Summer11*	0.2357
GMSB_Lambda-100_CTau-4000_7TeV_pythia6_cff/Summer11*	0.2357
GMSB_Lambda-100_CTau-6000_7TeV_pythia6_cff/Summer11*	0.2357
GMSB_Lambda-120_CTau-1_7TeV_pythia6_cff/Summer11*	0.0860
GMSB_Lambda-120_CTau-250_7TeV_pythia6_cff/Summer11*	0.0860
GMSB_Lambda-120_CTau-500_7TeV_pythia6_cff/Summer11*	0.0860
GMSB_Lambda-120_CTau-1000_7TeV_pythia6_cff/Summer11*	0.0860
GMSB_Lambda-120_CTau-2000_7TeV_pythia6_cff/Summer11*	0.0860
GMSB_Lambda-120_CTau-3000_7TeV_pythia6_cff/Summer11*	0.0860
GMSB_Lambda-120_CTau-4000_7TeV_pythia6_cff/Summer11*	0.0860
GMSB_Lambda-120_CTau-6000_7TeV_pythia6_cff/Summer11*	0.0860
GMSB_Lambda-140_CTau-1_7TeV_pythia6_cff/Summer11*	0.0368
GMSB_Lambda-140_CTau-250_7TeV_pythia6_cff/Summer11*	0.0368
GMSB_Lambda-140_CTau-500_7TeV_pythia6_cff/Summer11*	0.0368
GMSB_Lambda-140_CTau-1000_7TeV_pythia6_cff/Summer11*	0.0368
GMSB_Lambda-140_CTau-2000_7TeV_pythia6_cff/Summer11*	0.0368
GMSB_Lambda-140_CTau-3000_7TeV_pythia6_cff/Summer11*	0.0368
GMSB_Lambda-140_CTau-4000_7TeV_pythia6_cff/Summer11*	0.0368
GMSB_Lambda-140_CTau-6000_7TeV_pythia6_cff/Summer11*	0.0368
GMSB_Lambda-160_CTau-1_7TeV_pythia6_cff/Summer11*	0.0181
GMSB_Lambda-160_CTau-250_7TeV_pythia6_cff/Summer11*	0.0181
GMSB_Lambda-160_CTau-500_7TeV_pythia6_cff/Summer11*	0.0181
GMSB_Lambda-160_CTau-1000_7TeV_pythia6_cff/Summer11*	0.0181
GMSB_Lambda-160_CTau-2000_7TeV_pythia6_cff/Summer11*	0.0181
GMSB_Lambda-160_CTau-3000_7TeV_pythia6_cff/Summer11*	0.0181
GMSB_Lambda-160_CTau-4000_7TeV_pythia6_cff/Summer11*	0.0181
GMSB_Lambda-160_CTau-6000_7TeV_pythia6_cff/Summer11*	0.0181
GMSB_Lambda-180_CTau-1_7TeV_pythia6_cff/Summer11*	0.0092
GMSB_Lambda-180_CTau-250_7TeV_pythia6_cff/Summer11*	0.0092
GMSB_Lambda-180_CTau-500_7TeV_pythia6_cff/Summer11*	0.0092
GMSB_Lambda-180_CTau-1000_7TeV_pythia6_cff/Summer11*	0.0092
GMSB_Lambda-180_CTau-2000_7TeV_pythia6_cff/Summer11*	0.0092
GMSB_Lambda-180_CTau-3000_7TeV_pythia6_cff/Summer11*	0.0092
GMSB_Lambda-180_CTau-4000_7TeV_pythia6_cff/Summer11*	0.0092
GMSB_Lambda-180_CTau-6000_7TeV_pythia6_cff/Summer11*	0.0092

Table 7: Full description of the signal GMSB MC datasets used in this analysis

Dataset name
G_Pt-*_TuneZ2_7TeV_pythia6-Summer11-PU_S3-AODSIM
QCD_Pt-120to170_TuneZ2_7TeV_pythia6-Summer11-PU_S3-AODSIM
TT_TuneZ2_7TeV-pythia6-tauola-Summer11-PU_S3_START42_V11-v1-AODSIM
WToENu_TuneZ2_7TeV-pythia6-Summer11-PU_S3-AODSIM

Table 8: The description of the background MC samples used in this analysis